The spread of gap-junction mediated activity in neocortex is modulated by extracellular potassium

Christoforos A. Papasavvas[1], R. Ryley Parrish[1], and Andrew J. Trevelyan[1]

1. Institute of Neuroscience, Medical School, Framlington Place, Newcastle upon Tyne, NE2 4HH, UK.

Corresponding author: Andrew Trevelyan

Email: andrew.trevelyan@ncl.ac.uk

Short title: Gap-junction mediated activity in neocortex

Key words: Parvalbumin, interneurons, epilepsy, electrotonic, seizures

Table of contents category:

Pages: 18 Tables: 1 Figures: 7

Abstract: 248 words

Introduction: 346 words

Discussion: 493 words

Competing interests statement: The authors declare that they have no competing financial interests.

Abbreviations:

PV	Parvalbumin
ACSF	artificial cerebro-spinal fluid
NMDA	N-methyl-D-aspartate
AMPA	α-amino-3-hydroxy-5-methyl-4-isoxazolepropionic acid
APV	aminophosponovaleric acid
4-AP	4-aminopyridine

Abstract

Parvalbumin-expressing interneurons in cortical networks are coupled by gap-junctions, thus forming a syncytium that supports propagating epileptiform discharges, induced by blocking voltage-gated K^+ channels using 4-aminopyridine (4-AP). It remains unclear, however, whether these propagating events occur under more natural states, without pharmacological blockade. In particular, we investigated whether such propagation occurs when extracellular K^+ rises, as is known to occur following intense network activity, such as during seizures. We examined how increasing $[K^+]_o$ affects the likelihood of propagating activity away from a site of focal (200-400µm), optogenetic activation of PV-interneurons. Activity was recorded using a linear 16-electrode array placed along layer 5 of primary visual cortex. At baseline levels of $[K^+]_o$ (3.5mM), induced activity was recorded only within the illumination area. However, when $[K^+]_o$ was increased above a threshold level (50th percentile = 8.0mM; interquartile range = 7.5-9.5mM), time-locked activity was also recorded outside the illumination area, propagating at 59.1 +/- 16.6 mm/s. Blockade of glutamatergic synaptic transmission reduced the efficacy of propagation. Propagation was further reduced, and in most cases prevented altogether, by pharmacological blockade of gap-junctions, achieved by any of three different drugs, quinine, mefloquine or carbenoxolone. Wash-out of quinine rapidly re-established the pattern of propagating activity. We modelled these activity patterns to illustrate key qualitative differences between propagating discharges in high $[K^+]_o$ and 4-AP, arising from differences in the electrotonic effects of these two manipulations. We conclude that interneuronal syncytial interactions are likely to affect the complex electrographic dynamics of seizures, once $[K^+]_o$ is raised above this threshold level.

Introduction

Cortical interneurons are connected by gap-junctions to other interneurons within the same class (Galarreta & Hestrin, 1999; Gibson *et al.*, 1999; Galarreta & Hestrin, 2001; Amitai *et al.*, 2002; Hestrin & Galarreta, 2005; Juszczak & Swiergiel, 2009), providing a highly specific, excitatory link between these cells. Initial studies showed that gap-junction coupling normalised the voltage difference between two cells and further synchronised their firing with millisecond precision (Galarreta & Hestrin, 1999; Gibson *et al.*, 1999;

Bennett & Zukin, 2004; Connors & Long, 2004). These studies, however, only examined very localised sets of interneurons, and the question of how widely this synchronisation spreads is unresolved.

Propagation through this gap-junction coupled network has been observed in one particular pathological condition, in a widely used model of epileptic activity, induced by bathing brain slices in 4-aminopyridine (4-AP) (Szente *et al.*, 2002; Gajda *et al.*, 2003; Gigout *et al.*, 2006a). 4-AP blocks various voltage-dependent K^+ channels, and appears to have a disproportionate effect on the population of fast-spiking interneurons, inducing rhythmic bursting in these cells even in the absence of any glutamatergic drive (Avoli *et al.*, 2002; Bohannon & Hablitz, 2018; Parrish *et al.*, 2018). These epileptiform discharges propagate reliably across brain slices, with a broad and relatively slow wavefront. This though represents a rather specific case, in which the spread of activity through the syncytium is facilitated by two factors related to the K^+ conductance blockade, with cells being depolarised and also electrotonically more compact, and which may not occur *in vivo*. In contrast, we speculated that gap-junction mediated propagation may also be supported by a different change in the neuronal milieu, that has been demonstrated both *in vivo* and *in vitro*: namely, the raised extracellular potassium ($[K^+]_o$) associated with extreme levels of neuronal activity. We now show that this is indeed the case, although the pattern of spreading activity differs qualitatively from that seen in 4-AP. We used mice that express channelrhodopsin under the PV promoter, allowing us to stimulate specifically this population of interneurons in a highly focal manner. We then examined the time-locked activity propagating out from this focus of activation. We show that this propagation is sensitive to, but not dependent on, glutamatergic synaptic activity, but it is abolished by any of three different gap-junction blockers. We then explore the differences between the two patterns of spreading activity, induced either by high $[K^+]_o$ or 4-AP, using an extended, multi-neuron, compartmental model of the interneuronal syncytium.

Methods

Cortical expression of optogenetic proteins

All animal handling and experimentation were done according to the guidelines laid by the UK Home Office and Animals (Scientific Procedures) Act 1986 and approved by the

Newcastle University Animal Welfare and Ethical Review Body (AWERB # 545). Cortical channelrhodopsin-2 (ChR2) expression was achieved by using genetically engineered transgenic mice. Brain slices were prepared from first generation cross-breeding of homozygous floxed-channelrhodopsin mice (B6; 129S-Gt(ROSA)26Sortm32(CAG-COP4*H134R/EYFP)Hze/J; Jackson Laboratory, stock number 012569) with homozygous PV-cre mice (B6; 129P2-Pvalbtm1(cre)Arbr/J; Jackson Laboratory, stock number 008069).

Preparation of brain slices

Fifteen young mice (6-12 weeks old) were sacrificed to prepare the brain slices. They were first anesthetised using Ketamine (0.3 mL / 30 g) and then perfused with ice-cold sucrose-based artificial cerebrospinal fluid (ACSF: NaHCO3 24mM, KCl 3 mM, NaH2PO4 1.25 mM, sucrose 227.8 mM, glucose 10mM, MgCl2 4 mM) before the brain was removed to prepare coronal brain slices (400µm thick). The slices were cut on Leica VT1200 vibratome (Leica Microsystems, Wetzlar, Germany) in ice-cold oxygenated (95% O2/ 5% CO2) sucrose-based ACSF (NaCl 125mM, NaHCO3 26mM, glucose 10mM, KCl 3.5 mM, NaH2PO4 1.26 mM, MgCl2 3mM). After cutting, the slices were transferred to an incubation, interface chamber (room temperature) perfused with oxygenated (normal) ACSF (NaCl 125 mM, NaHCO3 26 mM, glucose 10 mM, KCl 3.5 mM, NaH2PO4 1.26 mM, CaCl2 2 mM, MgCl2 1 mM) for at least 1 hour before transferring them to a recording interface chamber. In the recording interface chamber, the ACSF used was normal ACSF as above. The ACSF was perfused at 1.5 2.5 ml /min and its temperature was kept at 33-36^{0}C. In the case of the ChR2 experiments, the concentration of extracellular K+ was systematically being increased during the recording by adding KCl to the perfused ACSF.

Extracellular recordings

Multichannel extracellular recordings were collected at 25 kHz unless otherwise stated, using a linear 16-channel-probe configuration (A16x1-2mm-100-177; NeuroNexus; electrode separation, 100 µm). This was connected to an ME16-FAI-µPA-system and MC-Rack software (Multichannel Systems, Reutlingen). Data acquisition was carried out using a 1401-3 Analog-Digital converter (Cambridge Electronic Design, Cambridge) and Spike2 software (Cambridge Electronic Design, Cambridge). The electrode array was placed along layer V in the occipital dorsal area of neocortex, approximately corresponding to primary visual cortex

(Dong, 2008). Channelrhodopsin was activated by a 470nm LED delivering light through the objective using the patterned illuminator Polygon400 (Mightex Systems, Pleasanton, CA, USA). The system was controlled and the patterns were designed through the PolyScan 2 software from the same company. The light intensity was measured at approximately 2 mW/mm^2

AMPA currents were blocked by bathing in 20 µM NBQX (HelloBio) and and NMDA currents were blocked using 50 µM d-APV (Abcam Biochemicals). We used three different gap junction blockers, namely Mefloquine (50 µM, Sigma-Aldrich, Gillingham, UK), Quinine (100 µM, Sigma-Aldrich, Gillingham, UK), Carbenoxolone (100 µM, Tocris Bioscience, Bristol, UK).

Simulations

The model cell consists of three compartments: one soma (27 µm length, 29 µm diameter, 1 segment) and two morphologically and biophysically identical dendrites (left and right; 200 µm length (Fukuda *et al.*, 2006), 0.8 µm diameter (Fukuda & Kosaka, 2003), 10 segments). The interneuron model used in this study is adapted from the biophysically detailed interneuron model from Konstantoudaki *et al.,* 2014 (ModelDB, Accession number: 168310). The soma is equipped with the following mechanisms: fast Na+ current, A-type K+ current, delayed-rectifier K+ current, slow K+ current, N-type high-threshold activated Ca++ current, hyperpolarization-activated cation current (Ih), fast afterhyperpolarization K+ current and a Ca++ buffering mechanism. The dendrites are equipped with the following mechanisms: fast Na+ current, A-type K+ current, and delayed-rectifier K+ current. The conductance values used are shown in Table 1. Seventy identical cells are scattered in a virtual slice with dimensions 650 µm x 150 µm x 150 µm. Thus, the density of the population is approximately 5 cells per volume of $(100\ \mu m)^3$ which is close to the density found in layer V of mouse primary visual cortex (Pakan *et al.*, 2016). The cells were randomly connected with gap junctions following the connectivity rule in Fig. 8B. A pair of cells would have a maximum of one gap junction (g_{gap} = 0.3nS; Fukuda *et al.*, 2006; Galarreta & Hestrin, 2002) connecting the right dendrite of the cell on the left with the left dendrite of the cell on the right. The placement of the gap junction along the dendrites was symmetric and was randomly placed with a uniform probability distribution between the closest point possible (considering the distance between the cells) and the full length of the dendrite. For

example: two cells with 100 µm distance between them could be connected from the 50 µm dendritic point away from their soma up to the most distal dendritic point, that is, 200 µm away from their soma.

The cells that were located in the leftmost 200 µm of the virtual slice were directly stimulated at the soma with a 25 ms pulse of 0.55 nA amplitude starting at 50ms into the simulation. The speed of propagation is calculated based on the first propagation wave, that is, the first spikes of two specific cells. It is equal to the distance travelled over time between the last cell in the stimulation area and the last cell in the overall propagation. For the results shown in Fig. 8E and 8F, only the first 200 long propagations were considered for the analysis. A long propagation is considered a propagation that reaches the 60th cell or beyond that.

All simulations were run using the NEURON simulator (Hines & Carnevale, 2001) through Python (PyNN interface (Davison *et al.*, 2008)).

Results

Optogenetic activation of parvalbumin-expressing cells

We investigated the propagation of activity through the syncytium of PV-expressing interneurons, in occipital cortical brain slices in different levels of extracellular K^+. Extracellular recordings were made from 53 mouse brain slices prepared from 22 young adult mice which expressed ChR2 under the PV promoter. We recorded extracellular field potentials using a linear multi-electrode array (MEA; 1.5 mm wide array of 16 electrodes with 0.1 mm spacing between the shafts) placed along layer 5 (Figure 1), where there is a dense network of electrically coupled PV-expressing interneurons (Galarreta & Hestrin, 1999; Gibson *et al.*, 1999; Fukuda & Kosaka, 2003). We optogenetically activated these PV-expressing interneurons specifically, in a small and circumscribed area, extending over 3-4 adjacent electrodes, using a focused patterned illuminator (400 x 100 µm, Figure 1 and Methods). The blue light was delivered as a train of pulses lasting 3s, at 20 Hz (50% duty cycle), and repeated every 20s. The spread of activity beyond the light spot was recorded using the linear multielectrode array, which typically extended at least 0.7 mm beyond the light spot, sampling at 100µm spaces between individual electrodes.

Propagation of activity with increased extracellular K^+

At baseline levels of extracellular K^+ ($[K^+]_o$ = 3.5mM), neuronal spiking was reliably recorded only at those electrodes within the spot of light. We then increased $[K^+]_o$, in increments of 1-2mM every 5 mins, to investigate how this affected activity patterns. Predictably, this produced a marked increase in spontaneous activity (Korn *et al.*, 1987; Jensen & Yaari, 1997), and additionally, in 43.4% of all brain slices (23 out of 53 brain slices) we also noted bursts of firing in electrodes away from the illumination site, that were time-locked, at short latencies, to the pattern of illumination. Thus, the raised extracellular $[K^+]$ facilitated the spread of activity away from the focal site of optogenetic activation (Figure 2), but tightly time-locked at short latencies, to the pulsed illumination. Notably, however, activity spreading beyond the focal illumination only occurred at higher levels of extracellular K^+. We measured the proportion of successful trials at different $[K^+]_o$ (Figure 3), which showed that the likelihood of propagation was strongly affected by $[K^+]_o$. Considering only those slices which showed propagation, we fitted a sigmoidal curve to this data, to derive the threshold level of $[K^+]_o$ supporting propagation (50% of trials). The threshold was 8.0 +/- 0.15 mM (median +/- 95% confidence interval; Interquartile range = 7.5-9.5mM; full range = 5.5-11.5mM).

Propagating activity was sensitive to glutamatergic and gap-junction blockers

We hypothesised that the propagating activity was spreading through gap-junction coupling which connects the population of PV-expressing interneurons. Examining only brain slices that showed clear propagation of activity beyond the illumination site (19 slices), and working at increased $[K^+]_o$ (mean = 8.45mM; range = 5.5-11.5mM), we first blocked glutamatergic currents using antagonists of AMPA and NMDA receptors (20µM NBQX and 50µM D-APV, respectively), to assess what contribution, if any, was made through conventional synaptic excitatory pathways. This also served to reduce the level of spontaneous activity. In a proportion of brain slices (6 out of 19 slices), following the introduction of glutamate blockers, the evoked propagating activity gradually diminished in parallel with the reduction in spontaneous activity, indicating that synaptic excitation did indeed contribute to these events. In the remaining brain slices (68.4% of slices), propagation of activity persisted, following glutamatergic blockade, and indeed was more apparent because it existed on a lower level of background activity.

We next assessed the effects of gap-junction blockers. Unfortunately, this class of drug shows off-target effects (Rozental *et al.*, 2001; Srinivas *et al.*, 2001; Cruikshank *et al.*, 2004), so we examined three different gap-junction blockers: mefloquine, quinine and carbenoxolone. In 3 out of 13 recordings, propagation persisted after the application of a gap junction blocker. In the remaining recordings (10/13 recordings = 76.9%), propagating activity was either abolished completely (9 cases) or the firing rate was decreased (65% decrease in 1 case), (Figures 4-5), and all three drugs showed this effect (quinine, n = 3; mefloquine, n = 6; carbenoxolone, n = 1). The example in Figure 4 shows the effect of quinine, but this pattern appears representative of the other drugs too, illustrating a rapid and marked decrease in both the amplitude and the firing rate of the recorded activity at electrodes away from the illumination site. Importantly, quinine (unlike the other drugs) can be washed out of the bath (Srinivas *et al.*, 2001), and when this was done, propagating activity was rapidly re-established (Figure 5). When a different gap-junction blocker, mefloquine (see Fig. 5 right panel), was then applied, this drug also blocked activity propagation. This recording further illustrated another principle, that glutamatergic activity did not sustain this pattern of propagation in the absence of gap-junction coupling.

We analysed the activity recorded across the multielectrode array with respect to the pulsed timing of the photostimulation (peri-stimulation spike histograms, Figure 6), in order to assess the propagation speed of the travelling wave of activity. The speed was calculated from the average latency of the first spikes at distal electrodes. We restricted our analyses only to those experiments where we had pharmacological confirmation of the involvement of gap-junctions (i.e. those using quinine, mefloquine or carbenoxolone). These had a median propagation speed of 59 mm/s and a spatial extent of up to 0.55 mm.

Simulating propagations through the PV-syncytium

The results presented above demonstrate that propagation through the PV-syncytium under conditions of raised extracellular K^+ is qualitatively different from that induced by 4-aminopyridine (Louvel *et al.*, 2001; Gigout *et al.*, 2006a; Gigout *et al.*, 2006b). In raised $[K^+]_o$, propagation was significantly faster (59mm/s) than in 4AP (15mm/s) (Gigout *et al.*, 2006a). There were further differences in the characteristics of the local field potential: in 4AP, activity had a large low frequency component, indicative of synchronous activity of many cells, and a broad wave-front. In high $[K^+]_o$, on the other hand, propagation is manifested as

unit activity (single action potentials from isolated cells). As such, the spread of activity in raised $[K^+]_o$ is more sparse, and is prone to failures of propagation, as evidence from the reduced extent of the propagating activity in this model (up to 0.55 mm), compared to 4AP (> 2mm (Gigout *et al.*, 2006a)).

In order to understand these differences better, we developed simulations of biophysically detailed cells that are connected through gap junctions in a 3-dimensional virtual slice. In particular, we were keen to assess how the difference in the cellular electrotonic properties in the two cases impacted on the spread. In both cases, neurons are depolarised relative to baseline, but for different reasons: in high $[K^+]_o$, because the K^+ reversal potential is relatively depolarised, and in 4-AP, because there is a reduced K^+ conductance. A further difference is that in 4-AP, the blockade of K^+ channels will additionally reduce the membrane conductivity, meaning that neurons are more electrotonically compact, thus further facilitating spread through the gap-junctions.

We modelled each neuron as a simple, three compartment model, with a soma and two 200µm-long dendrites (see Fig. 7A). Seventy of these cells were uniformly scattered in a 3-dimensional virtual slice, and randomly connected through gap junctions located on their dendrites (Fig. 7A-B). Each cell had a 'left' and 'right' dendrite, and its connectivity with the rest of the network was dictated by its location on the x-axis, such that each dendrite only connected to other neurons on that side. This imposed directionality to the network, so when the left part of the virtual slice is stimulated, the activity propagated from left to right. The cell index increased linearly from side of stimulation (left, id = 1; right, id = 70). The connectivity matrix in Fig. 7C shows an example of a randomly connected network, that follows the connectivity rule in Fig. 7B, and shows that the leftmost cells do not have a direct connection with the rightmost cells.

Cells located in the left-most 200µm of the virtual slice were stimulated 50ms after starting the simulation, and the stimulation pulse, delivered directly to their soma, lasted for 25ms. The exact number of cells stimulated varied slightly from simulation to simulation since the scattering of the cells in the virtual slice was random. Simulations were run for each one of the three cases: (a) control case, where the settings are set to default; (b) high K^+ case, where the extracellular potassium concentration is considered to be raised to 10.5mM, instead of the default 3.5mM; and (c) 4-AP case, where the membrane resistance is five times higher than the default value and the K^+ channels are blocked, that is, their

conductance is set to 2% of their default value. Typical results of these simulations are shown in Fig. 7D for each one of the different cases. The blue regions in the scatter plots represent the temporal and spatial extend of the stimulation. For the control case, only the cells in the stimulation area were active, and this activity did not spread beyond the stimulation area at all. In the high $[K^+]_o$ case, activity propagated beyond the area of stimulation, but typically failed before the end of the slice (i.e., 70th cell). Furthermore, we found that even within the propagating territory, the wave of activity could skip some neurons, since there are multiple paths across the network. Thus, not all cells are participating in the propagation. Interestingly, the propagation did not advance smoothly. Rather, following stimulation, there was a rapid and almost simultaneous activation of a group of cells in the middle of the slice, followed by a delay before the next set of neurons were recruited.

Gap-junction mediated propagation in the 4-AP simulations, though, were qualitatively different. There was a more gradual and slow propagation that reliably reached the end of the slice without failing. The participation of the cells was complete, with few, if any, being skipped during the propagation (median = 100% as opposed to 71.1% for high $[K^+]_o$ simulations; $p << 0.001$, two-sided Wilcoxon rank sum test; Figure 7F). The distribution of the propagation speeds in 200 simulations for each case is shown in Fig. 8E. The median propagation speed for the high K^+ case is 57.1 mm/s. This value is close to what was expected from the experimental results presented above. The median propagation speed of the 4AP case is significantly lower (33.5 mm/s; $p << 0.001$, two-sided Wilcoxon rank sum test) but higher than the expected one from previous studies (15mm/s) (Gigout *et al.*, 2006a).

Discussion

Previously, several groups have demonstrated propagating interneuronal discharges, induced by 4-AP in cortical networks, and which are mediated through gap-junction coupling between the interneuronal populations (Szente *et al.*, 2002; Gajda *et al.*, 2003; Gigout *et al.*, 2006a). This pharmacological manipulation, while of interest, does represent a rather extreme disruption of neocortical interneuron behaviour (Codadu *et al.*, 2019a). Of particular relevance to the present study is that 4-AP makes neurons more electrotonically

compact, by blocking a large component of K^+ conductance, and will thus naturally facilitate electrotonic propagation. Of wider relevance is the state of raised $[K^+]_o$, which is thought to occur whenever there is intense neuronal activation, and is thus likely to occur during all seizures (for an extensive review of this literature, see (Somjen, 2004)). Since 4-AP has a disproportionately large effect on the population of parvalbumin-expressing interneurons (Codadu *et al.*, 2019a), we also chose to study the effect of raised $[K^+]_o$ in this same population. Electrical coupling between this population of interneurons is well established (Galarreta & Hestrin, 2001; Hestrin & Galarreta, 2005), but coupling has also been described for other populations of cortical interneurons, and our findings are likely to generalise to these neuronal populations too.

One notable finding is that the pattern of gap-junction coupled propagation in high $[K^+]_o$, where we see tightly time-locked and rapid propagation of single action potentials, appears different from that in 4-AP, which takes the form of a broad wave-front, with a relatively small high frequency component (e.g. (Gigout *et al.*, 2006a; Gigout *et al.*, 2006b; Parrish *et al.*, 2018) A further distinction between these two experimental paradigms is that 4-AP waves additionally involve other interneuronal populations, and may also trigger waves of raised $[K^+]_o$ themselves, secondary to GABAergic induced chloride-loading (Viitanen *et al.*, 2010), both of which would be expected to broaden the wave.

The primary effect of enhancing the electrical coupling of interneurons in this way, will be to extend the inhibitory surround during focal cortical activation (Prince & Wilder, 1967; Schwartz & Bonhoeffer, 2001; Trevelyan *et al.*, 2006; Parrish *et al.*, 2019), while also enhancing coordination of this inhibitory effect. Interneuronal activity at this time, however, is a double edged sword, because there is now good evidence that these neurons may become active drivers of epileptic discharges, if pyramidal cells become loaded with chloride (Huberfeld *et al.*, 2007; Dzhala *et al.*, 2010; Avoli & de Curtis, 2011; Ellender *et al.*, 2014; Pallud *et al.*, 2014; Alfonsa *et al.*, 2015; Raimondo *et al.*, 2015; Alfonsa *et al.*, 2016)(Chang *et al.*, 2018). Raised extracellular K^+ will also facilitate chloride loading, which is coupled via the cation-chloride co-transporter, KCC2. In either case, whether GABAergic output is inhibitory or excitatory, the enhanced coupling of interneurons through their gap-junctions is likely to be an important determinant of the complex pattern of propagating local field potentials during a seizure (Viventi *et al.*, 2011; Smith *et al.*, 2016; Codadu *et al.*, 2019b). It is also highly pertinent that gap-junction expression is commonly increased in

epileptic brains (Manjarrez-Marmolejo & Franco-Perez, 2016). Whether this is protective, or serves to exacerbate the epileptic condition, remains an open question.

Figure legends

Figure 1. Schematic of the experimental setup and the equipment used. (A) Extracellular recordings were taken using a linear multi-electrode array (MEA) placed along layer V in a cortical slice where ChR2 was expressed in PV^+ cells. The photostimulation (blue LED) was delivered using a patterned illuminator through the objective. (B) Schematic of the linear 16-electrode array used in the experiments. The image was taken from the NeuroNexus catalogue (A16x1-2mm-100-177). Note that the distance between adjacent electrodes is 100 µm. (C) The recordings were taken from the dorsal area of the slice, targeting the primary visual area. (D) Example of an illumination pattern which was drawn in the middle of the array. This illumination was limited to a 4-electrode wide area (from the 6th to the 9th).

Figure 2. Propagating activity arising with raised extracellular K^+. The area around a subset of the electrodes is illuminated (marked with blue) with 3-second long pulse trains (20Hz, 50% duty cycle) which repeat every 15 s. PV^+ cells around these electrodes are responding with 4-5 spikes per pulse (see zoom-in traces). After raising the extracellular K^+ concentration (from 3.5mM to 7.5mM), induced activity is recorded in a distant electrode as well (150µm away). The activity recorded outside the illumination area is time-locked to the activity inside that area and it is recorded with some delay. Considering that the photostimulated cells are GABAergic in nature, the activity at the distant electrode is hypothesized to propagate through the electrical synapses between PV^+ cells.

Figure 3. Concentration of extracellular K^+ needed to observe propagation of activity. The plot shows the cumulative proportion of detected propagations at different levels of extracellular K^+ concentration. The majority of propagations (15 out of 23, 65.2%) were observed with an increase of the extracellular K^+ up to 8.5 mM. The threshold (at the 50% point) was calculated at 8.0 mM after fitting a sigmoidal function (red dashed curve).

Figure 4. Pharmacological manipulation of the propagating activity. The underlying mechanisms of the propagating activity were investigated by the application of pharmacological agents. This example is the continuation of the example in Figure 2. First, the glutamate receptors were blocked by applying NBQX and D-APV (left panel). In this example, the spontaneous activity was decreased but the propagated activity at the distant electrode remained strong. This indicates that glutamate release (e.g., through disinhibition) was not involved in the propagation. Then, the gap junction blocker quinine was applied (right panel). The activity recorded 250 µm away was gradually suppressed and silenced as evidenced by the decreasing amplitude and spike rate.

Figure 5. Validating the implication of gap junctions by applying multiple gap junction blockers. The propagating activity silenced in Fig. 4 was recovered by washing out the blockers (left panel). Stable propagating activity with increasing amplitude was recovered at the electrode 350 µm away. This activity remained strong for several minutes until another gap junction blocker was applied, namely mefloquine (right panel). The propagating activity was once again blocked validating the involvement of gap junctions by using two different blockers.

Figure 6. Calculating the speed of propagation. (A) Example of how the speed of propagation was calculated. The spike time histograms from two different electrodes were plotted: one inside the illumination area (close to the border) and one outside the illumination area where propagating activity was detected. The period covered by the histogram matches the period of the illumination pulse. The first peak in each histogram was detected (marked by asterisks). The propagation speed was directly calculated from the time difference between these peaks and the known distance between the electrodes. (B) The distribution of the calculated propagation speeds reveals high variability (standard deviation 16.6mm/s) and a median speed of 59.1mm/s. This plot includes only the propagations that were shown to be mediated by the gap junctions.

Figure 7: Simulation of the high K+ propagation and comparison with the 4AP propagation (A) Schematic of the model cell and of the model network of electrically connected cells. The cell has a simple morphology with a soma and two dendrites, one on the left and one on the right. The cells are randomly placed in a 3-dimensional virtual slice and they form a

network through gap junctions. The left dendrite for each cell is used to connect it with other cells located on its left whereas the right dendrite is used to connect it with cells on the right. The left side of the network is stimulated and the activity propagates to the right. (B) The probability of connection between two cells is linearly decreased as the distance between them increases. (C) Example of a connectivity matrix of a randomly generated network where the yellow colour indicates a connection. The cell id is derived from the ordering of the cells on the x-axis, from left to right. Notice that the leftmost cells do to have any direct connection with the rightmost cells due to the limited length of their dendrite (200 µm). (D) Typical results of the simulation under three conditions: control, high K+, and 4AP. In the control case there is no propagation; only the cells in the stimulation area fire. In the high K+ case, there is a fast propagation to the right side of the network but not all cells are participating. In the 4AP case, there is qualitatively different propagation where the speed is lower but almost every cell in the network participates. (E) Distribution of propagation speeds for the high K+ and 4AP cases. The propagation under high K+ conditions is significantly faster ($p << 0.001$, two-sided Wilcoxon rank sum test). (F) Distribution of participation percentages for the high K+ and 4AP cases. The participation under 4AP conditions is significantly higher ($p << 0.001$, two-sided Wilcoxon rank sum test).

Table 1: Biophysical mechanisms used in the model and their conductance values

References

Alfonsa, H., Lakey, J.H., Lightowlers, R.N. & Trevelyan, A.J. (2016) Cl-out is a novel cooperative optogenetic tool for extruding chloride from neurons. *Nature communications*, **7**, 13495.

Alfonsa, H., Merricks, E.M., Codadu, N.K., Cunningham, M.O., Deisseroth, K., Racca, C. & Trevelyan, A.J. (2015) The contribution of raised intraneuronal chloride to epileptic network activity. *J Neurosci*, **35**, 7715-7726.

Amitai, Y., Gibson, J.R., Beierlein, M., Patrick, S.L., Ho, A.M., Connors, B.W. & Golomb, D. (2002) The spatial dimensions of electrically coupled networks of interneurons in the neocortex. *J Neurosci*, **22**, 4142-4152.

Avoli, M., D'Antuono, M., Louvel, J., Kohling, R., Biagini, G., Pumain, R., D'Arcangelo, G. & Tancredi, V. (2002) Network and pharmacological mechanisms leading to epileptiform synchronization in the limbic system in vitro. *Prog Neurobiol*, **68**, 167-207.

Avoli, M. & de Curtis, M. (2011) GABAergic synchronization in the limbic system and its role in the generation of epileptiform activity. *Prog Neurobiol*, **95**, 104-132.

Bennett, M.V. & Zukin, R.S. (2004) Electrical coupling and neuronal synchronization in the Mammalian brain. *Neuron*, **41**, 495-511.

Bohannon, A.S. & Hablitz, J.J. (2018) Optogenetic dissection of roles of specific cortical interneuron subtypes in GABAergic network synchronization. *J Physiol*, **596**, 901-919.

Chang, M., Dian, J.A., Dufour, S., Wang, L., Moradi Chameh, H., Ramani, M., Zhang, L., Carlen, P.L., Womelsdorf, T. & Valiante, T.A. (2018) Brief activation of GABAergic interneurons initiates the transition to ictal events through post-inhibitory rebound excitation. *Neurobiol Dis*, **109**, 102-116.

Codadu, N.K., Graham, R.T., Burman, R.J., Jackson-Taylor, R.T., Raimondo, J.V., Trevelyan, A.J. & Parrish, R.R. (2019a) Divergent paths to seizure-like events. http://www.biorxiv.org/content/10.1101/641530v1.

Codadu, N.K., Parrish, R.R. & Trevelyan, A.J. (2019b) Region-specific differences and areal interactions underlying transitions in epileptiform activity. *J Physiol*.

Connors, B.W. & Long, M.A. (2004) Electrical synapses in the mammalian brain. *Annu Rev Neurosci*, **27**, 393-418.

Cruikshank, S.J., Hopperstad, M., Younger, M., Connors, B.W., Spray, D.C. & Srinivas, M. (2004) Potent block of Cx36 and Cx50 gap junction channels by mefloquine. *Proc Natl Acad Sci U S A*, **101**, 12364-12369.

Davison, A.P., Bruderle, D., Eppler, J., Kremkow, J., Muller, E., Pecevski, D., Perrinet, L. & Yger, P. (2008) PyNN: A Common Interface for Neuronal Network Simulators. *Frontiers in neuroinformatics*, **2**, 11.

Dong, H.W. (2008) *Allen reference atlas : a digital color brain atlas of the C57Black/6J male mouse*. Wiley, Hoboken, N.J.

Dzhala, V.I., Kuchibhotla, K.V., Glykys, J.C., Kahle, K.T., Swiercz, W.B., Feng, G., Kuner, T., Augustine, G.J., Bacskai, B.J. & Staley, K.J. (2010) Progressive NKCC1-dependent

neuronal chloride accumulation during neonatal seizures. *J Neurosci*, **30**, 11745-11761.

Ellender, T.J., Raimondo, J.V., Irkle, A., Lamsa, K.P. & Akerman, C.J. (2014) Excitatory effects of parvalbumin-expressing interneurons maintain hippocampal epileptiform activity via synchronous afterdischarges. *J Neurosci*, **34**, 15208-15222.

Fukuda, T. & Kosaka, T. (2003) Ultrastructural study of gap junctions between dendrites of parvalbumin-containing GABAergic neurons in various neocortical areas of the adult rat. *Neuroscience*, **120**, 5-20.

Fukuda, T., Kosaka, T., Singer W. & Galuske R.A.W. (2006) Gap Junctions among Dendrites of Cortical GABAergic Neurons Establish a Dense and Widespread Intercolumnar Network. *J Neurosci,* **26**, 3434–3443.

Gajda, Z., Gyengesi, E., Hermesz, E., Ali, K.S. & Szente, M. (2003) Involvement of gap junctions in the manifestation and control of the duration of seizures in rats in vivo. *Epilepsia*, **44**, 1596-1600.

Galarreta, M. & Hestrin, S. (1999) A network of fast-spiking cells in the neocortex connected by electrical synapses. *Nature*, **402**, 72-75.

Galarreta, M. & Hestrin, S. (2001) Spike transmission and synchrony detection in networks of GABAergic interneurons. *Science*, **292**, 2295-2299.

Galarreta, M. & Hestrin, S. (2002). Electrical and chemical synapses among parvalbumin fast-spiking GABAergic interneurons in adult mouse neocortex. *Proc Natl Acad Sci U S A*, **99**, 12438–12443.

Gibson, J.R., Beierlein, M. & Connors, B.W. (1999) Two networks of electrically coupled inhibitory neurons in neocortex. *Nature*, **402**, 75-79.

Gigout, S., Louvel, J., Kawasaki, H., D'Antuono, M., Armand, V., Kurcewicz, I., Olivier, A., Laschet, J., Turak, B., Devaux, B., Pumain, R. & Avoli, M. (2006a) Effects of gap junction blockers on human neocortical synchronization. *Neurobiol Dis*, **22**, 496-508.

Gigout, S., Louvel, J. & Pumain, R. (2006b) Effects in vitro and in vivo of a gap junction blocker on epileptiform activities in a genetic model of absence epilepsy. *Epilepsy Res*, **69**, 15-29.

Hestrin, S. & Galarreta, M. (2005) Electrical synapses define networks of neocortical GABAergic neurons. *Trends Neurosci*, **28**, 304-309.

Hines, M.L. & Carnevale, N.T. (2001) NEURON: a tool for neuroscientists. *Neuroscientist*, **7**, 123-135.

Huberfeld, G., Wittner, L., Clemenceau, S., Baulac, M., Kaila, K., Miles, R. & Rivera, C. (2007) Perturbed chloride homeostasis and GABAergic signaling in human temporal lobe epilepsy. *J Neurosci*, **27**, 9866-9873.

Jensen, M.S. & Yaari, Y. (1997) Role of intrinsic burst firing, potassium accumulation, and electrical coupling in the elevated potassium model of hippocampal epilepsy. *J Neurophysiol*, **77**, 1224-1233.

Juszczak, G.R. & Swiergiel, A.H. (2009) Properties of gap junction blockers and their behavioural, cognitive and electrophysiological effects: animal and human studies. *Prog Neuropsychopharmacol Biol Psychiatry*, **33**, 181-198.

Korn, S.J., Giacchino, J.L., Chamberlin, N.L. & Dingledine, R. (1987) Epileptiform burst activity induced by potassium in the hippocampus and its regulation by GABA-mediated inhibition. *J Neurophysiol*, **57**, 325-340.

Louvel, J., Papatheodoropoulos, C., Siniscalchi, A., Kurcewicz, I., Pumain, R., Devaux, B., Turak, B., Esposito, V., Villemeure, J.G. & Avoli, M. (2001) GABA-mediated synchronization in the human neocortex: elevations in extracellular potassium and presynaptic mechanisms. *Neuroscience*, **105**, 803-813.

Manjarrez-Marmolejo, J. & Franco-Perez, J. (2016) Gap Junction Blockers: An Overview of their Effects on Induced Seizures in Animal Models. *Current neuropharmacology*, **14**, 759-771.

Pakan, J.M., Lowe, S.C., Dylda, E., Keemink, S.W., Currie, S.P., Coutts, C.A. & Rochefort, N.L. (2016). Behavioral-state modulation of inhibition is context-dependent and cell type specific in mouse visual cortex. *Elife,* **5**, 7250–7257.

Pallud, J., Le Van Quyen, M., Bielle, F., Pellegrino, C., Varlet, P., Labussiere, M., Cresto, N., Dieme, M.J., Baulac, M., Duyckaerts, C., Kourdougli, N., Chazal, G., Devaux, B., Rivera, C., Miles, R., Capelle, L. & Huberfeld, G. (2014) Cortical GABAergic excitation contributes to epileptic activities around human glioma. *Science translational medicine*, **6**, 244ra289.

Parrish, R.R., Codadu, N.K., Racca, C. & Trevelyan, A.J. (2018) Pyramidal cell activity levels affect the polarity of gene transciption changes in interneurons. *J Neurophysiol*, **120**, 2358–2367.

Parrish, R.R., Codadu, N.K., Scott, C.M. & Trevelyan, A.J. (2019) Feedforward inhibition ahead of ictal wavefronts is provided by both parvalbumin and somatostatin expressing interneurons. *J Physiol*.

Prince, D.A. & Wilder, B.J. (1967) Control mechanisms in cortical epileptogenic foci. "Surround" inhibition. *Arch Neurol*, **16**, 194-202.

Raimondo, J.V., Burman, R.J., Katz, A.A. & Akerman, C.J. (2015) Ion dynamics during seizures. *Frontiers in cellular neuroscience*, **9**, 419.

Rozental, R., Srinivas, M. & Spray, D.C. (2001) How to close a gap junction channel. Efficacies and potencies of uncoupling agents. *Methods in molecular biology*, **154**, 447-476.

Schwartz, T.H. & Bonhoeffer, T. (2001) In vivo optical mapping of epileptic foci and surround inhibition in ferret cerebral cortex. *Nat Med*, **7**, 1063-1067.

Smith, E.H., Liou, J.Y., Davis, T.S., Merricks, E.M., Kellis, S.S., Weiss, S.A., Greger, B., House, P.A., McKhann Ii, G.M., Goodman, R.R., Emerson, R.G., Bateman, L.M., Trevelyan, A.J. & Schevon, C.A. (2016) The ictal wavefront is the spatiotemporal source of discharges during spontaneous human seizures. *Nature communications*, **7**, 11098.

Somjen, G.G. (2004) *Ions in the brain: Normal function, seizures and stroke*. Oxford University Press, Oxford.

Srinivas, M., Hopperstad, M.G. & Spray, D.C. (2001) Quinine blocks specific gap junction channel subtypes. *Proc Natl Acad Sci U S A*, **98**, 10942-10947.

Szente, M., Gajda, Z., Said Ali, K. & Hermesz, E. (2002) Involvement of electrical coupling in the in vivo ictal epileptiform activity induced by 4-aminopyridine in the neocortex. *Neuroscience*, **115**, 1067-1078.

Trevelyan, A.J., Sussillo, D., Watson, B.O. & Yuste, R. (2006) Modular propagation of epileptiform activity: evidence for an inhibitory veto in neocortex. *J Neurosci*, **26**, 12447-12455.

Viitanen, T., Ruusuvuori, E., Kaila, K. & Voipio, J. (2010) The K+-Cl cotransporter KCC2 promotes GABAergic excitation in the mature rat hippocampus. *J Physiol*, **588**, 1527-1540.

Viventi, J., Kim, D.H., Vigeland, L., Frechette, E.S., Blanco, J.A., Kim, Y.S., Avrin, A.E., Tiruvadi, V.R., Hwang, S.W., Vanleer, A.C., Wulsin, D.F., Davis, K., Gelber, C.E., Palmer, L., Van der Spiegel, J., Wu, J., Xiao, J., Huang, Y., Contreras, D., Rogers, J.A. & Litt, B. (2011) Flexible, foldable, actively multiplexed, high-density electrode array for mapping brain activity in vivo. *Nat Neurosci*, **14**, 1599-1605.

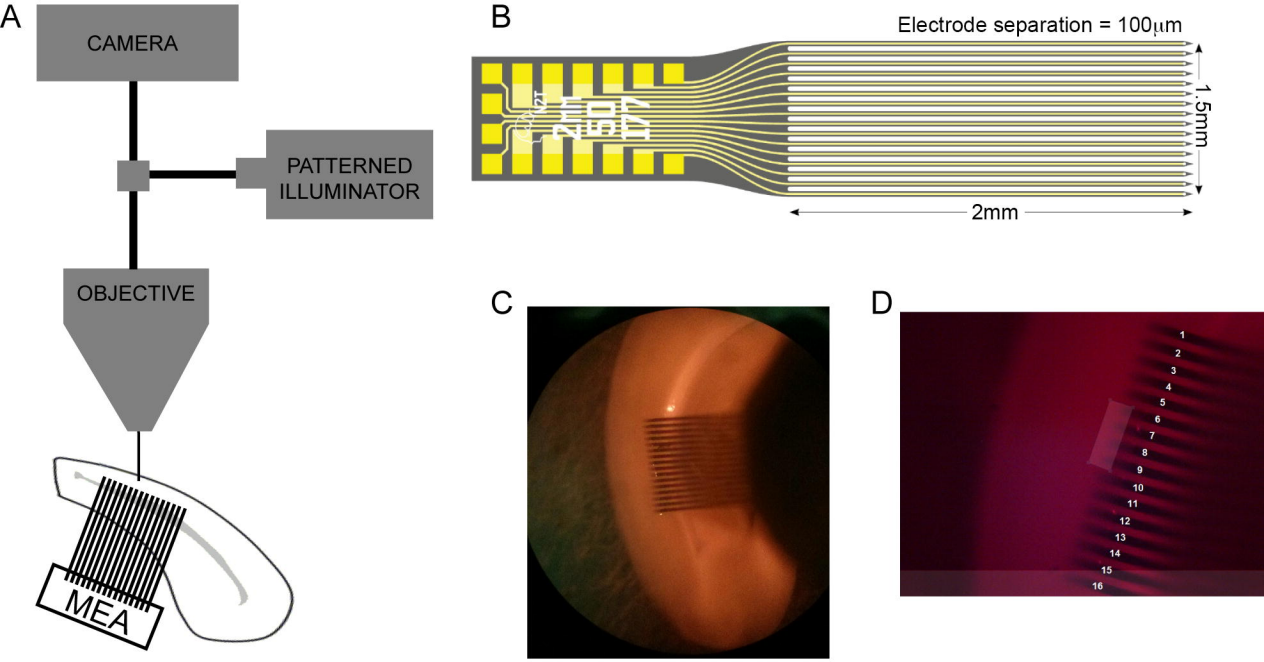
A
CAMERA
PATTERNED ILLUMINATOR
OBJECTIVE
MEA
B
Electrode separation = 100μm
1.5mm
2mm
C
D
1
2
3
4
5
6
7
8
9
10
11
12
13
14
15
16

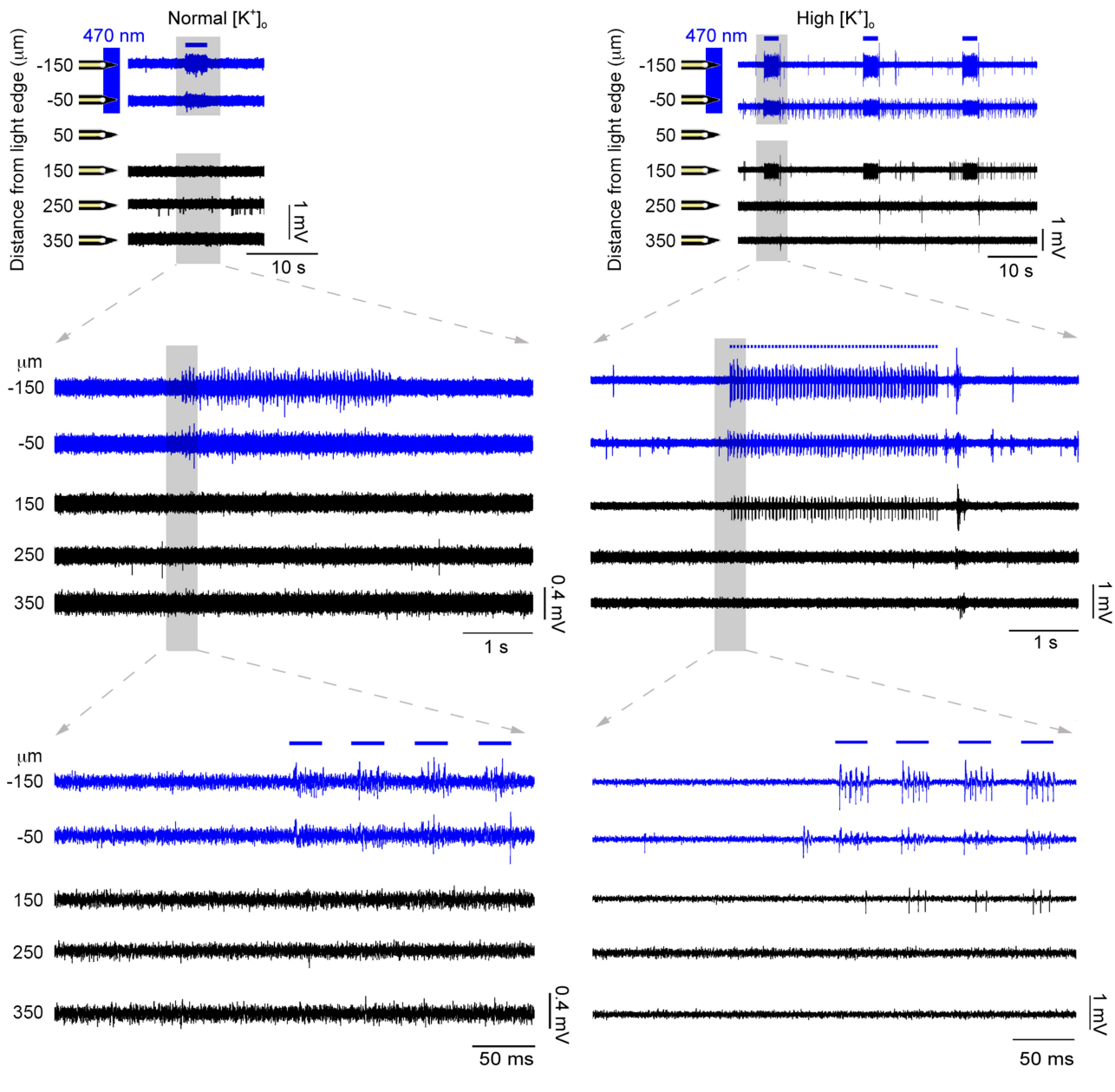
Normal [K+]o
High [K+]o
470 nm
Distance from light edge (µm)
-150
-50
50
150
250
350
1 mV
10 s
µm
0.4 mV
1 s
50 ms

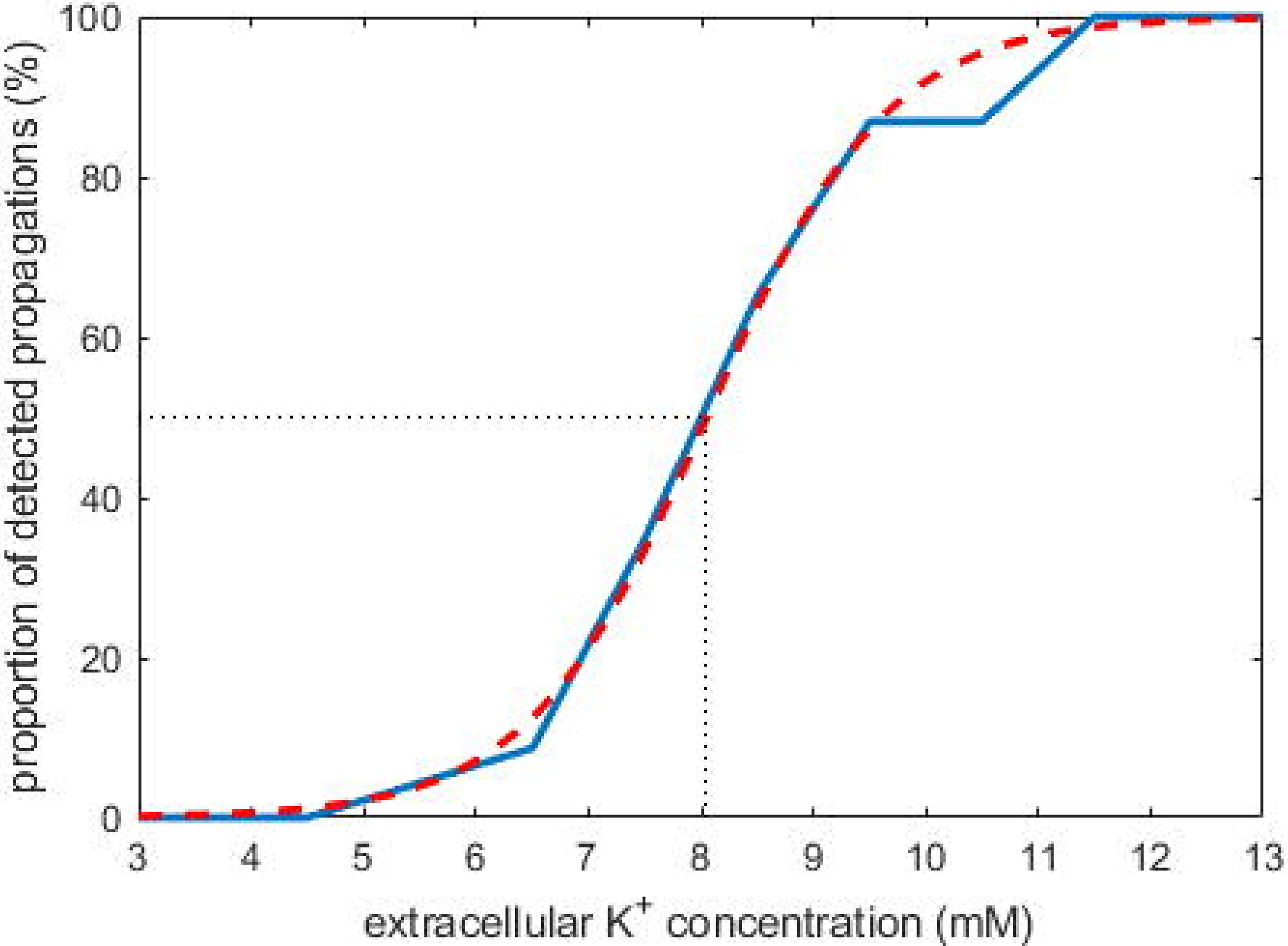
100
80
60
40
20
0
proportion of detected propagations (%)
3
4
5
6
7
8
9
10
11
12
13
extracellular K+ concentration (mM)

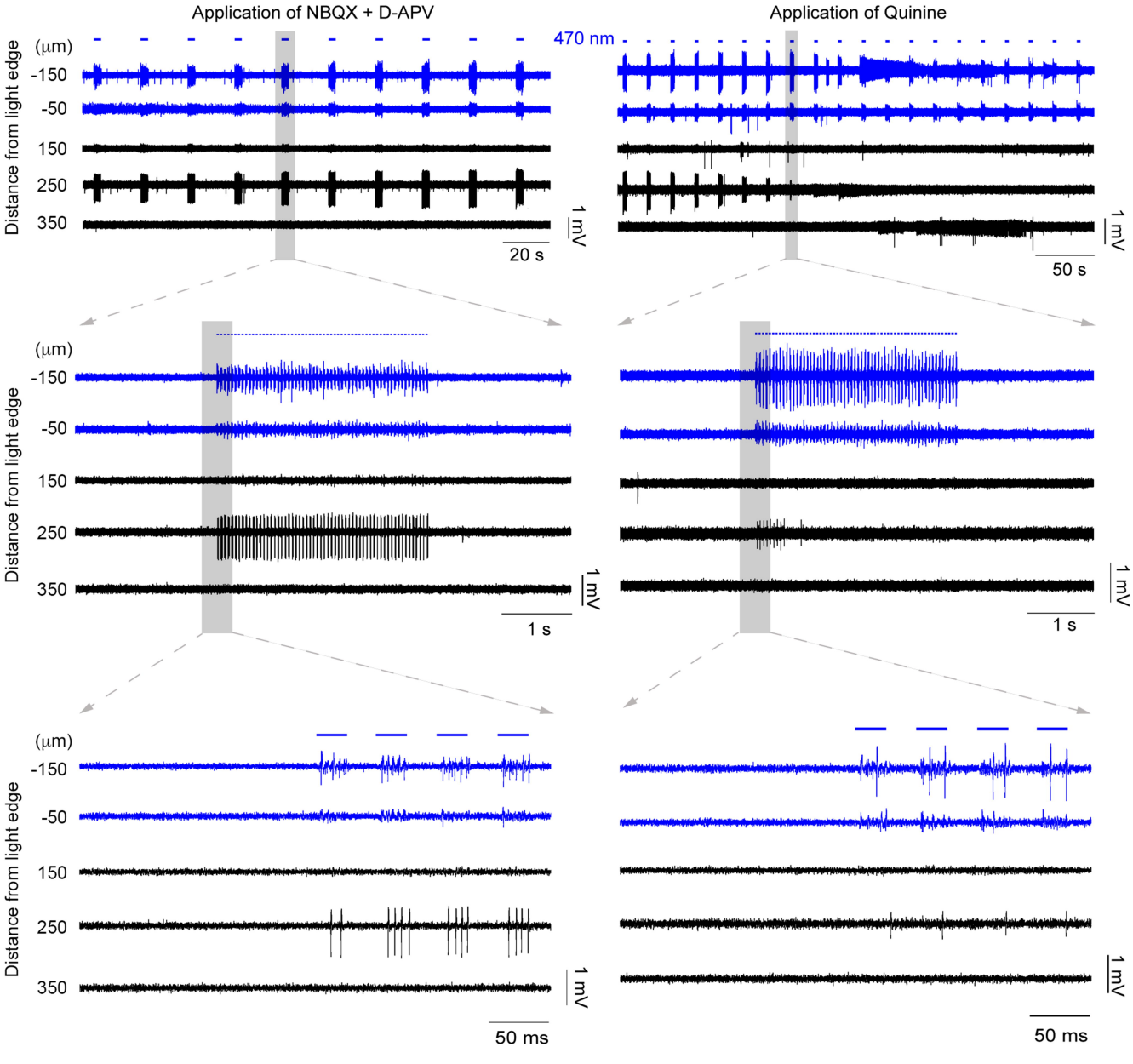
Application of NBQX + D-APV
Application of Quinine
470 nm
(µm)
Distance from light edge
-150
-50
150
250
350
1 mV
20 s
50 s
1 s
50 ms

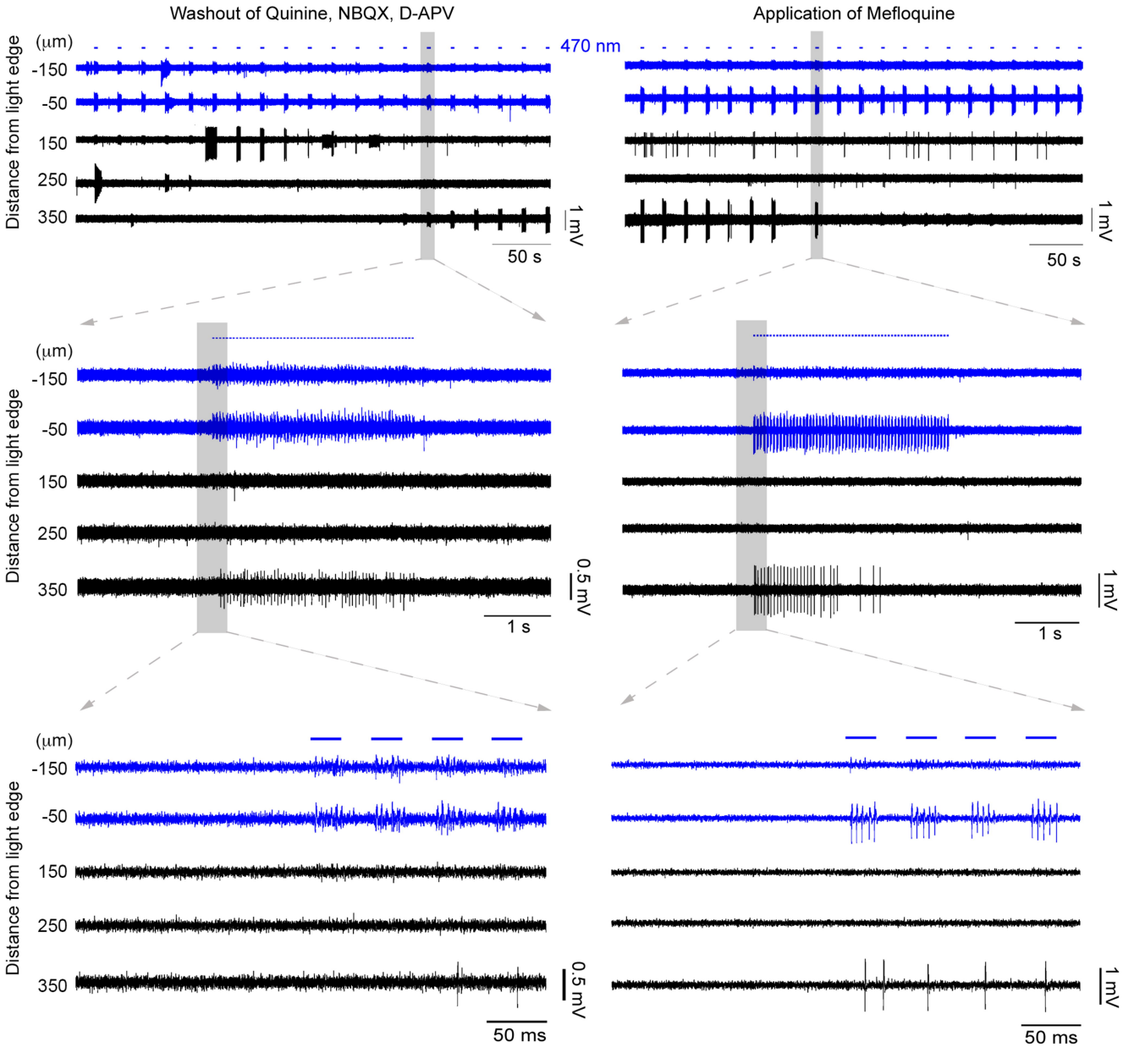
Washout of Quinine, NBQX, D-APV
Application of Mefloquine
470 nm
(μm)
Distance from light edge
-150
-50
150
250
350
1 mV
50 s
0.5 mV
1 s
50 ms

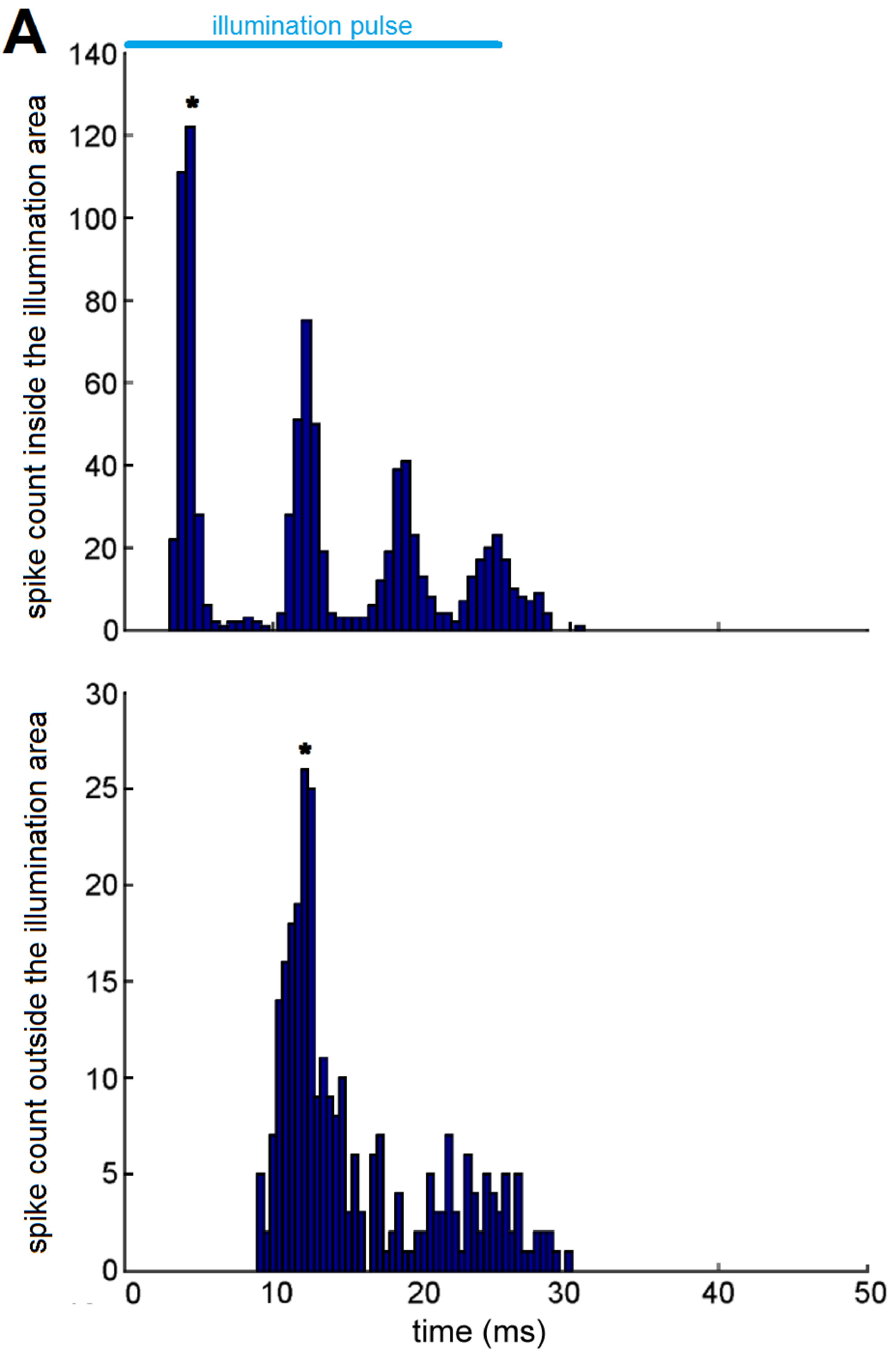
A
illumination pulse
spike count inside the illumination area
140
120
100
80
60
40
20
0
*
spike count outside the illumination area
30
25
20
15
10
5
0
*
0
10
20
30
40
50
time (ms)

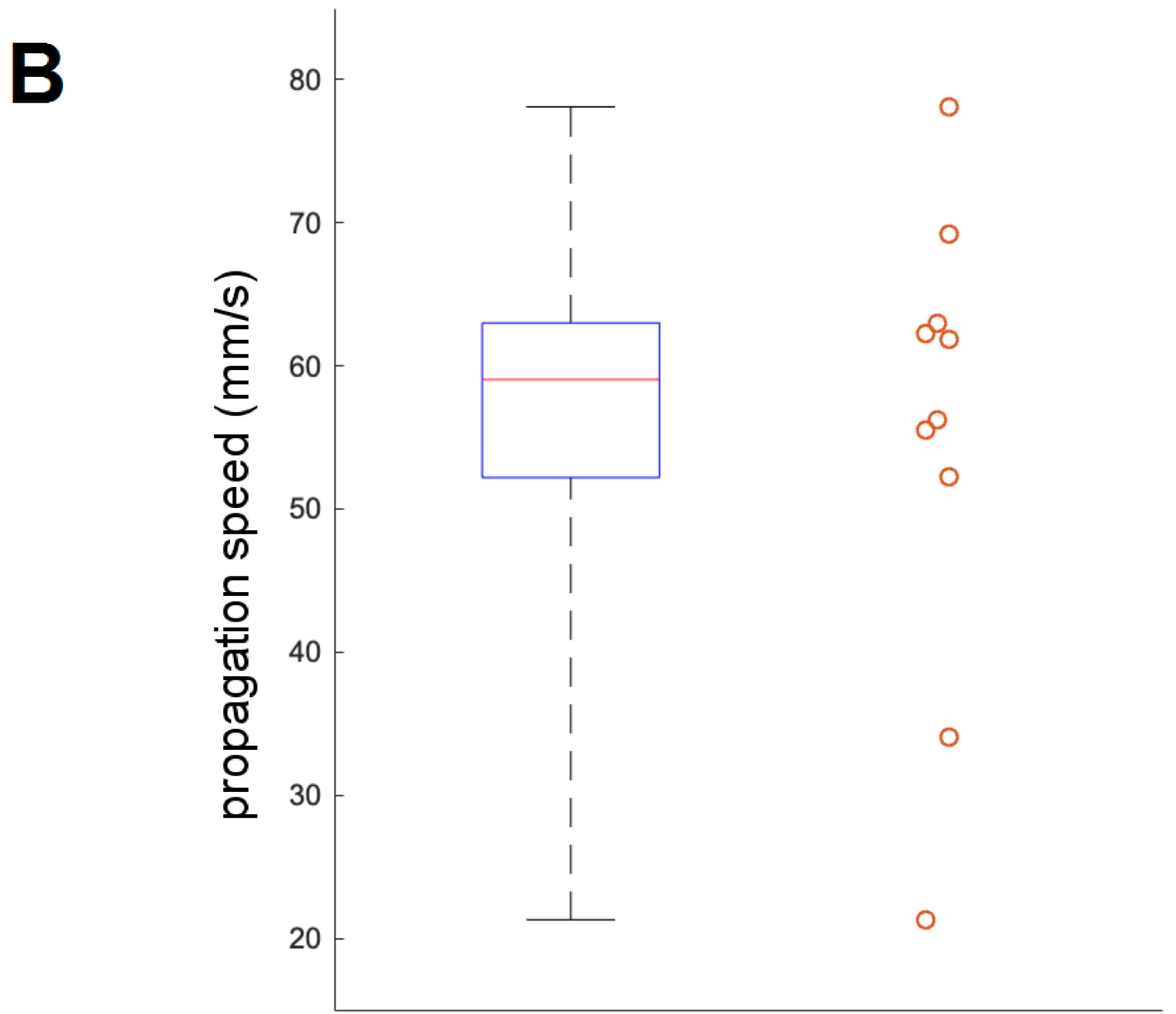
B
propagation speed (mm/s)
80
70
60
50
40
30
20

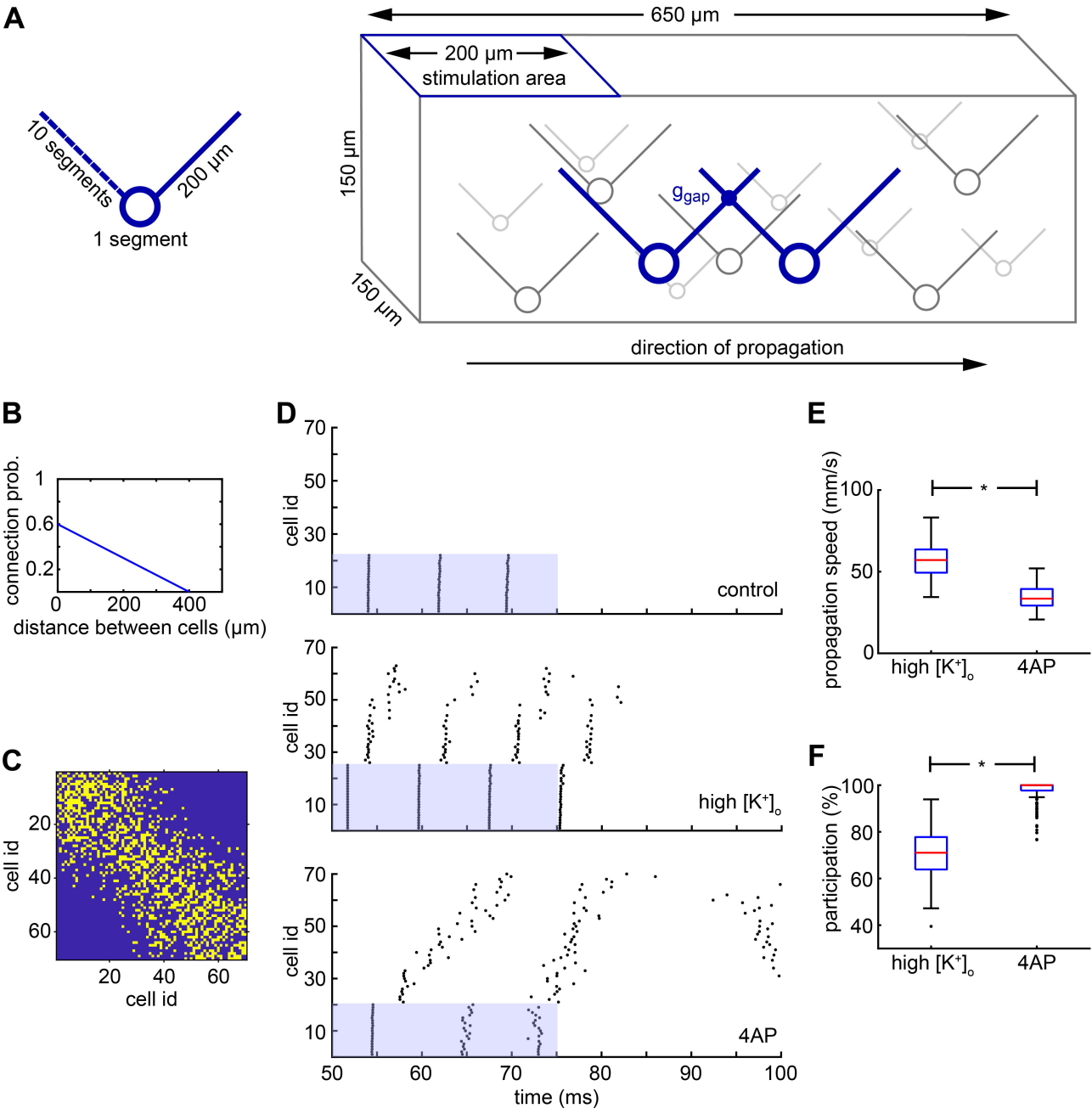
A
650 µm
200 µm
stimulation area
150 µm
150 µm
10 segments
200 µm
1 segment
g_{gap}
direction of propagation
B
connection prob.
1
0.6
0.2
0
200
400
distance between cells (µm)
C
cell id
20
40
60
20
40
60
cell id
D
cell id
70
50
30
10
control
high $[K^+]_o$
4AP
50
60
70
80
90
100
time (ms)
E
propagation speed (mm/s)
100
50
0
*
high $[K^+]_o$
4AP
F
participation (%)
100
80
60
40
*
high $[K^+]_o$
4AP

mechanism	soma	dendrite
Na^+ conductance (S/cm^2)	0.045	0.06
Delayed rectifier K^+	0.018	0.009
N-type Ca^{++}	0.0003	N/A
D-type K^+	0.0000725	N/A
H-current	0.00001	N/A
A-type K^+	0.048	0.48
fAHP	0.0001	N/A
Ca^{++} diffusion	yes	no
Cm ($\mu F/cm^2$)	1.2	1.2
Ra (ohm/cm)	150	150
Rm (kOhm cm^2)	10	10